Chemical Engineering Journal 334 (2018) 508–518

Contents lists available at ScienceDirect

Chemical Engineering Journal

journal homepage: www.elsevier.com/locate/cej

Insight into the kinetics and mechanism of removal of aqueous chlorinated nitroaromatic antibiotic chloramphenicol by nanoscale zero-valent iron

Xue Liu[a], Zhen Cao[a], Zilin Yuan[b], Jing Zhang[a], Xingpan Guo[a], Yi Yang[a], Feng He[c,*], Yaping Zhao[d], Jiang Xu[a,b,*]

[a] State Key Laboratory of Estuarine and Coastal Research, East China Normal University, Shanghai 200062, China
[b] Department of Civil and Environmental Engineering, Carnegie Mellon University, Pittsburgh 15213, USA
[c] College of Environment, Zhejiang University of Technology, Hangzhou 310014, China
[d] School of Ecological and Environmental Science, East China Normal University, Shanghai 200241, China

GRAPHICAL ABSTRACT

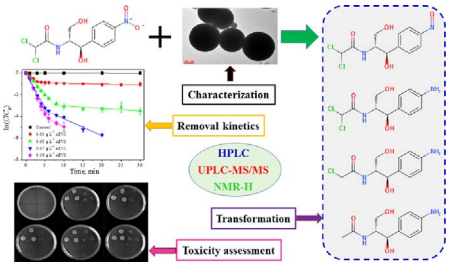

ARTICLE INFO

Keywords:
Nanoscale zero-valent iron
Chloramphenicol
Removal
Kinetics
Mechanism
Antibacterial activity

ABSTRACT

Nanoscale zero-valent iron (nZVI) is very efficient in removing chlorinated nitroaromatic antibiotic chloramphenicol (CAP) from different waters including DI water, surface water, groundwater, and seawater. The corrosion of nZVI and product distribution after reaction in these water matrices were also investigated. Based on the identification of four main reduction products via HPLC, UPLC-MS/MS, and NMR-H spectrums, a more detailed pathway of CAP degradation by nZVI was proposed than ever reported. The two O atoms on the NO_2 group were successively reduced first, and then two Cl atoms were removed via dechlorination. The process of CAP removal could be divided into two stages according to the pseudo-first-order kinetic model. A total of 97.0% of 0.30 mM CAP was rapidly removed by 1.8 mM nZVI in the first stage (6 min) with a surface-area-normalized reaction rate of 1.13 L min^{-1} m^{-2}. Notably, after reaction with nZVI, the antibacterial activity of the CAP solution was greatly reduced. This study demonstrates that nZVI is a promising alternative to remediate CAP-contaminated water to reduce the antibiotic selection pressure of the environment.

1. Introduction

Widespread attention has been paid to water pollution from emerging organic contaminants (EOCs), which are broadly regarded as newly generated or detected naturally occurring compounds and synthetic chemicals that are not controlled by legislation [1]. As a special category of EOCs, antibiotics in water and food have become an emerging issue due to their threats to ecosystems and human health via the generation of antibiotic-resistant bacteria and genes [2,3]. Chloramphenicol (CAP), a chlorinated nitroaromatic antibiotic, is an effective bacteriostatic pharmaceutical that has been applied in a large scale since its first application in clinical practice in 1949. Although its use

* Corresponding authors at: State Key Laboratory of Estuarine and Coastal Research, East China Normal University, Shanghai 200062, China (J. Xu).
E-mail addresses: fenghe@zjut.edu.cn (F. He), jiangx2@andrew.cmu.edu (J. Xu).

http://dx.doi.org/10.1016/j.cej.2017.10.060
Received 16 June 2017; Received in revised form 9 October 2017; Accepted 13 October 2017
Available online 16 October 2017
1385-8947/

has been banned in many countries, it is still used in many developing nations due to its wide availability and low production costs. China is the largest producer and consumer of antibiotics, such as CAP. The existence and frequent detection of CAP in sewage influent and effluent, as well as surface and underground water in China, have been reported in previous studies by ourselves and others [4–7]. The concentration of CAP in municipal sewage, river water, and river sediment in Guiyang City in China was reported to be up to 47.4 μg L^{-1}, 19.0 μg L^{-1}, and 1138 μg kg^{-1}, respectively [8].

Various technologies have been developed to remove antibiotics from water, including adsorption, photo-degradation, catalytic oxidation, biodegradation, and microwave radiation [9–14]. Nanoscale zero valent iron (nZVI) is a useful nanomaterial that can remove a wide range of pollutants, including nitrate, heavy metals, and organics because of its large surface area and strong activity [15–21]. The use of nZVI has been proposed as a new strategy to remove non-biodegradable organic pollutants via adsorption and reduction, thereby eliminating the functional groups on the pollutant, decreasing the toxicity, and increasing the biodegradability, especially for halogenated organics pollution [22–25]. The antibiotic properties of CAP are greatly influenced by the NO_2 functional group on the CAP molecule, and the antibiotic characteristic can be effectively decreased via the reduction of nitroaromatics to aromatic amines, which are less toxic and more readily biodegradable [26,27]. Similar effects are also expected after dechlorination of CAP. However, only two degradation products of CAP by nZVI were detected by LC-MS in previous studies [28,29] and the detailed CAP degradation pathway remains unclear. Whether or not and to what extent the reduction of CAP by nZVI reduces solution toxicity remains unknown. In addition, current limited studies on CAP removal by nZVI were all performed in DI waters and its performance in real water matrices remains to be investigated.

The primary objective of this study is to investigate the removal of CAP by nZVI with a focus on the degradation pathway and toxicity change. The specific objectives are: (1) to study the kinetics of CAP removal by nZVI in DI water and natural waters; (2) to investigate the effects of solution chemistry on CAP removal; (3) to elucidate the degradation pathway of CAP by nZVI and discuss the reaction mechanism through nZVI characterization before and after reaction; and (4) to assess the toxicity change of the organics before and after reaction.

2. Experimental section

2.1. Chemicals

Analytical grade chemicals, including $NaBH_4$, $FeSO_4{\cdot}7H_2O$, NaCl, NaOH, and HCl, were purchased from the Sinopharm Group Chemical Reagent Co., Ltd., China. CAP was obtained from Aladdin Reagent (Shanghai) Co., Ltd. DI water (pH = 7.0) was purged by nitrogen for 1 h prior to use in nZVI preparation and batch experiments. All chemicals were used without further purification.

2.2. Preparation of nZVI

The entire preparation procedure was performed in a 1000 mL three-necked flask that was located in a thermostatic water bath. Briefly, 0.25 g $FeSO_4$ $7H_2O$ was dissolved in a flask with 200 mL DI water purged of nitrogen, and a stoichiometric amount of 200 mL $NaBH_4$ (0.07 g) solution was added dropwise and mechanically stirred at 500 rpm to generate nZVI (0.05 g) according to the following equation [30]:

$$Fe^{2+} + 2BH_4^- + 6H_2O \rightarrow Fe + 2B(OH)_3 + 7H_2 \quad (1)$$

2.3. Batch experiments

Batch experiments were all performed under nitrogen flow in 1000 mL three-necked flasks containing 500 mL freshly prepared nZVI and CAP DI water solution. Unless otherwise specified, the reaction between 1.8 mM nZVI and 0.30 mM CAP was carried out under mechanical stirring at 500 rpm, pH = 7.0, and 303 K. Samples were collected at specified times, and the reaction was quenched after filtration through a 0.45 μm polyether sulfone (PES) membrane. CAP removal due to filter sorption was negligible (Fig. S1). The cytotoxicity of the reaction solution was assessed using *E. coli*, which is presented with details in Supporting Information.

Experiments were also carried out with nitrogen purging using four different natural waters, including groundwater (collected from a well in Shandong Province), river water (collected from Suzhou River in Shanghai), seawater (collected from the Yellow Sea in Shandong Province), and wastewater (collected from the secondary effluent of a wastewater treatment plant in Shanghai). A total of 1.8 mM nZVI and 0.30 mM CAP were added for testing.

2.4. Analytical methods

CAP in the filtered aqueous samples were analyzed by HPLC (Agilent 1260 Infinity), and the analysis of the reaction products was carried out using a UPLC-MS/MS system, including a Waters Acquity UPLC system coupled with electrospray ionization and a Waters Quattro Premier quadrupole tandem mass spectrometer. Detailed detection methods are presented in the Supporting Information.

Field emission scanning electron microscopy (SEM, FEI-Quanta 200F), energy dispersive X-ray spectroscopy (EDX, FEI-Quanta 200F), transmission electron microscopy (TEM, FEI-Tecnai G^2 F20), X-ray diffraction (XRD, Rigaku-Ultima IV), X-ray photoelectron spectroscopy (XPS, Thermo Scientific K-Alpha), Brunauer-Emmett-Teller (BET, Quantachrome 02108-KR-1), and a Zeta potential meter (Malvern Nano-ZS90) were used to characterize the nZVI.

3. Results and discussion

3.1. Characterization of nZVI

The morphologies of the nZVI particles before and after reaction with CAP were compared using SEM and TEM with the same magnification. The fresh nZVI (6.52 m^2 g^{-1}) showed a chain-like aggregation of smooth and spherical particles (Fig. 1a and c). However, the nZVI particles became rougher and smaller with the appearance of flocculent substances after the reaction (Fig. 1b and d). This change was also indicated by the particle's increased specific surface area (17.78 m^2 g^{-1}). In TEM images with higher magnification (Fig. 1e and f), a core-shell structure was clearly observed. The fresh nZVI particles were enclosed within a thin shell of several nanometers [31]. The shell became much thicker after reaction, indicating that a portion of the nZVI was consumed and iron (hydr)oxides were produced during the reaction.

Fig. 2a shows the XRD patterns of nZVI. The peak appeared at 2θ = 44.9° was the typical Fe^0 peak [32], and peaks corresponding to iron oxides were not observed before the reaction. Since the oxidation of nZVI is inevitable as shown in the EDX spectra (Fig. S2), the absence of iron oxide peaks suggest that their percentage is below detection limits. After reaction, new peaks appeared at 2θ = 31°/36°/57°/62.5°, which are corresponding to Fe_2O_3 and Fe_3O_4, indicating the generation or increase of these oxides. The much weakened peak at 44.9° suggests that Fe^0 was significantly consumed but still present in the residual particles.

XPS analysis was performed to study the changes of Fe chemical states before and after reaction (Fig. 2b). Narrow scans of the Fe 2p XPS spectra of nZVI before reaction (Fig. 2c) showed that Fe was mainly in forms of Fe^0 (centered at 706.9/719.7 eV), FeO (centered at 710.5 eV), Fe_2O_3 (centered at 710.8/724.5 eV), and Fe_3O_4 (centered at 712.2 eV). The peaks of Fe^0 were weaker than those of iron oxides because XPS analysis usually provides superficial information on nanoparticles by

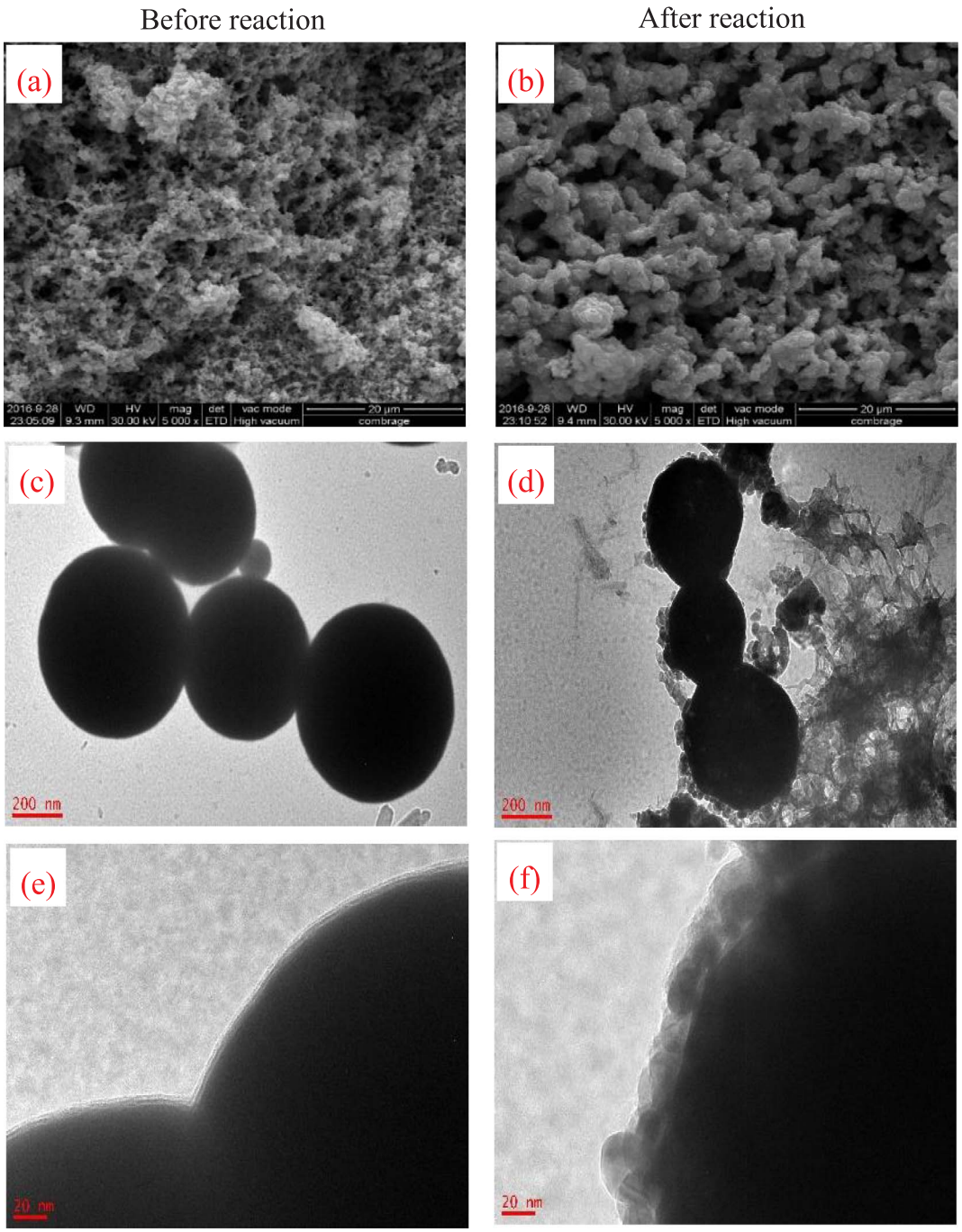

Fig. 1. (a, b) SEM and (c–f) TEM images of nZVI before and after the reaction.

using soft X-ray, which only has a detection depth of several nanometers [33]. However, Fe^0 was not observed in the XPS spectra of reacted nZVI (Fig. 2d), indicated the increased thickness of the oxide layer.

3.2. Product analysis and possible mechanism of CAP removal by nZVI

In order to elucidate the entire pathway of CAP removal by nZVI, UPLC-MS/MS analysis was performed to detect the reduction products of CAP by nZVI. Figs. S3 and S4 presents selected chromatographs from the UPLC-MS/MS analysis, where five typical peaks at retention times of approximately 9.34 min, 9.33 min, 3.91 min, 3.59 min, and 2.92 min were observed. Relative mass spectrums were analyzed to obtain the molecular weights (MWs) of the products, and detailed mass spectrums from the UPLC-MS/MS analysis are shown in Figs. S5–S8, which clearly describe the changes in CAP and its reduction products during the reaction.

Table 1 summarizes the possible reduction products based on the results of UPLC-MS/MS analysis, and from this, the mechanism of CAP removal by nZVI is proposed (Fig. 3). First, the O atom connected with the N atom via the coordination bond in the NO_2 group on CAP was chemically reduced by nZVI, generating an intermediate product detected at retention time of 9.33 min with a MW of 307 (CAP − O). This product was quickly produced and then degraded within several minutes (Figs. S5 and S9), which was the main reason for the rapid removal of CAP in the first stage. Then, the other O atom on the nitro group was

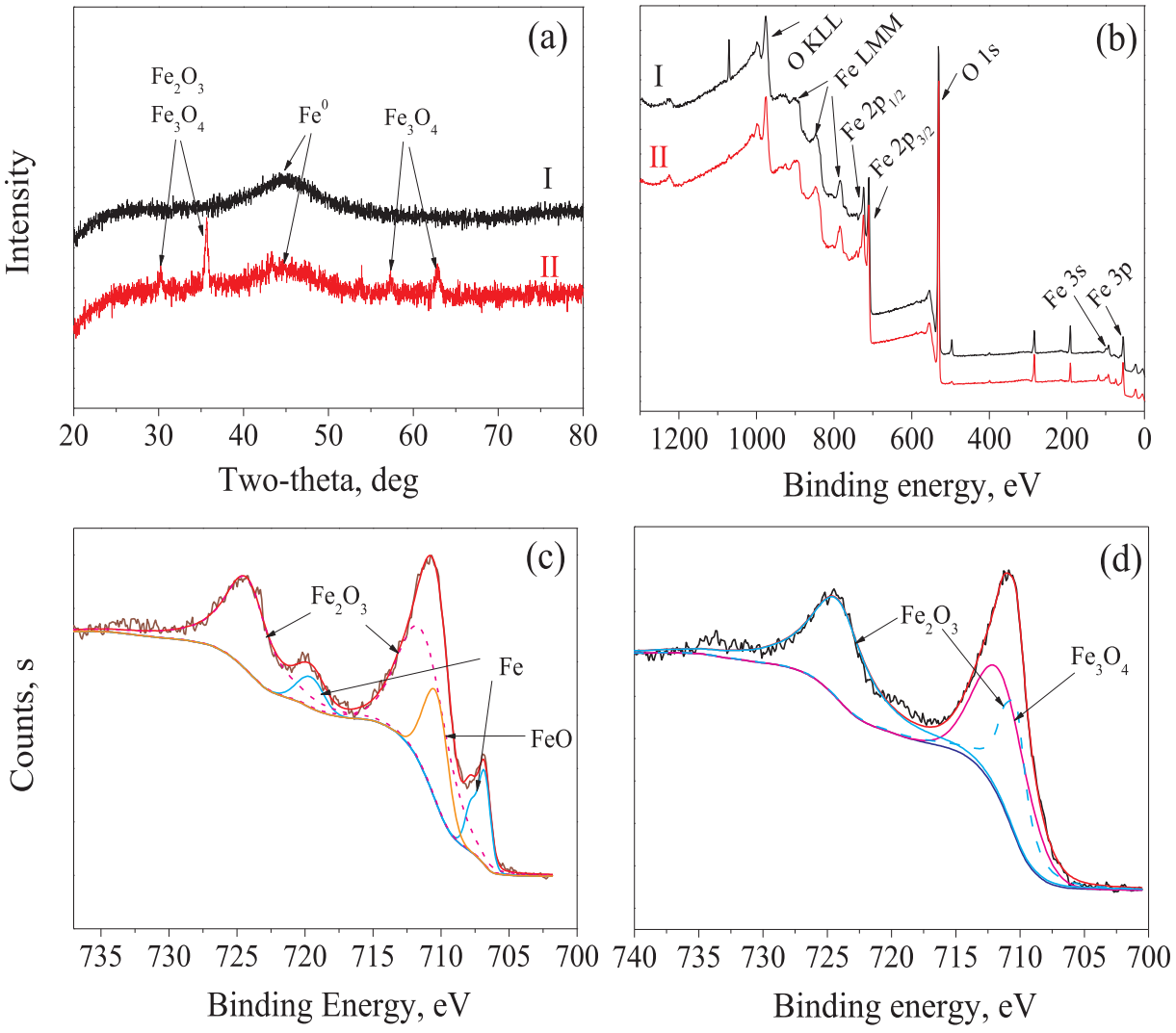

Fig. 2. (a) XRD and (b) XPS spectra of nZVI before (curve I) and after (curve II) the reaction; narrow scans of Fe 2p XPS spectra of nZVI (c) before and (d) after the reaction.

Table 1
Potential products of CAP removal by nZVI via UPLC-MS/MS.

Compound	Retention time (min)	MW	Molecular formula	Potential structure
CAP	9.34	323	$C_{11}H_{12}Cl_2N_2O_5$	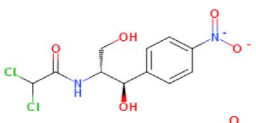
CAP − O	9.33	307	$C_{11}H_{12}Cl_2N_2O_4$	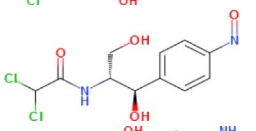
CAP − 2O	3.91	293	$C_{11}H_{14}Cl_2N_2O_3$	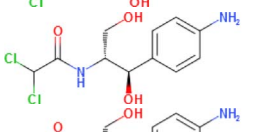
CAP − 2O − Cl	3.59	259	$C_{11}H_{15}ClN_2O_3$	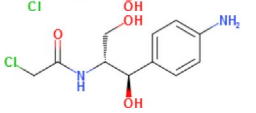
CAP − 2O − 2Cl	2.92	224	$C_{11}H_{16}N_2O_3$	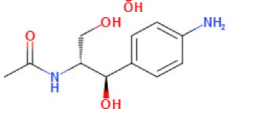

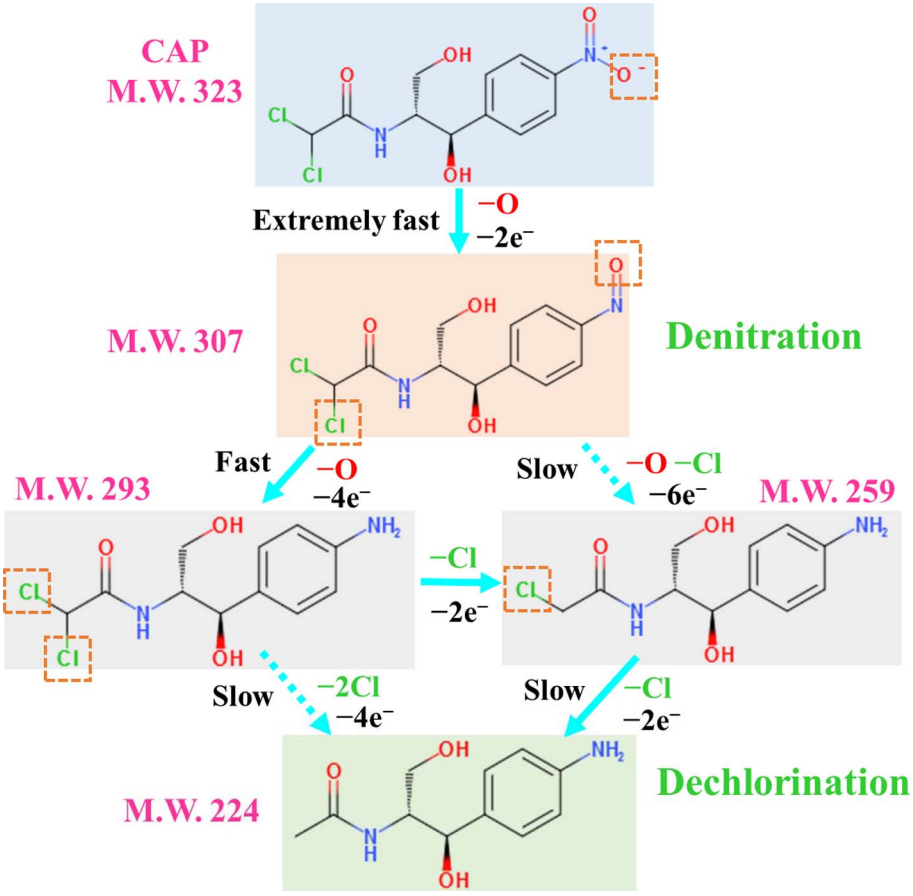

Fig. 3. Schematic of the mechanism of CAP removal by nZVI.

removed. At this time, the NO_2 group was completely reduced and converted to NH_2 group. This change was inferred via the peaks at 3.91 min with a MW of 293 (CAP − 2O). As the reaction proceeded, one Cl atom was further removed via dechlorination to form another compound, as suggested by the peaks at 3.59 min with a MW of 259 (CAP − 2O − Cl). The thoroughly dechlorinated product (MW: 224, CAP − 2O − 2Cl) was detected by UPLC-MS/MS after 40 min of reaction (Fig. S8). The low yield of CAP − 2O − 2Cl indicated that the reduction of CAP − 2O − Cl by nZVI was not efficient enough. Moreover, two substances were isolated from the reaction solution after 5 min and 20 min via silica gel column chromatography separation, respectively, which were confirmed to be CAP − O and CAP − 2O, respectively, according to the NMR-H spectrums (Fig. S10).

3.3. Kinetics of CAP removal by nZVI

The reaction kinetics of the removal of CAP by nZVI are described by a pseudo-first-order kinetic model that has been widely used to describe the removal of conventional and emerging organic contaminants by nZVI [34–39].

$$dC/dt = -k_{obs}C = -k_{SA}a_s\rho_m C \quad (2)$$

$$\ln(C_t/C_0) = -k_{obs}t \quad (3)$$

$$t_{1/2} = (\ln 2)/k_{obs} \quad (4)$$

where C_0 (mg L^{-1}) and C_t (mg L^{-1}) is the concentration of aqueous CAP at time 0 and t (min), respectively; k_{obs} (min^{-1}) stands for the observed removal rate constant of CAP by nZVI; k_{SA} is the surface-area-normalized reaction rate (L min^{-1} m^{-2}), a_s is the specific surface area of nZVI (m^2 g^{-1}), and ρ_m is the mass concentration of nZVI (g L^{-1}); $t_{1/2}$ is the half-life calculated from the first-order decay fitting using k_{obs}.

Based on the plots of $\ln(C_t/C_0)$ against t shown in Fig. 4, it was obvious that in most cases, the removal process of CAP by nZVI could be divided into two stages. In the first stage, the concentration of aqueous CAP sharply decreased, which suggested the strong reactivity of nZVI. The data on CAP removal by nZVI in the first stage were well fitted by the pseudo-first-order kinetics (Eqs. (2) and (3)), and the average values of the corresponding correlation coefficients (R^2) were as high as 0.994. The values of k_{obs}, k_{SA}, $t_{1/2}$, and R^2 for the removal of CAP by nZVI are summarized in Table 2. Generally, the removal rate of CAP by nZVI was very high, and half of the CAP could be removed by nZVI within 1 min under the primary reaction conditions. In the second stage, the removal was slower than in the first stage, as indicated by the smaller slope of the linear relationship between $\ln(C_t/C_0)$ and t. The retarded CAP removal is likely a result of the growth of a passive iron hydro(oxide)s layer on nZVI surface as evidenced in the TEM image (Fig. 1d and f), which inhibits the electron transfer from the Fe^0 core to CAP adsorbed on nZVI surface.

3.3.1. Effects of nZVI dosage and initial CAP concentration

The dosages of the initial reactants (nZVI and CAP) are important parameters that affect the reaction. As shown in Fig. 4a, a control experiment was performed without nZVI, and almost no CAP was reduced, while the increased removal of CAP was observed with the increased nZVI. Generally, the reduction of CAP to the primary intermediate (CAP − O) and final product (CAP − 2O − 2Cl) requires 2 e^- and 10 e^- per molar, respectively. Hence, the reduction of 0.30 mM CAP to CAP − O and CAP − 2O − 2Cl in this study requires at least 0.30 mM and 1.50 mM Fe^0, respectively, assuming Fe^0 provides 2 e^- to form Fe^{2+} under our reaction conditions (i.e., anoxic). Since all the Fe^0 in nZVI that synthesized from sodium borohydride reduction of ferrous iron was accessible under iron-limited conditions [40], the reason for no removal of CAP in the second stage by 0.5 mM nZVI was attributed to the exhaustion of Fe^0. While at higher dosage of nZVI (i.e. 1.8 mM),

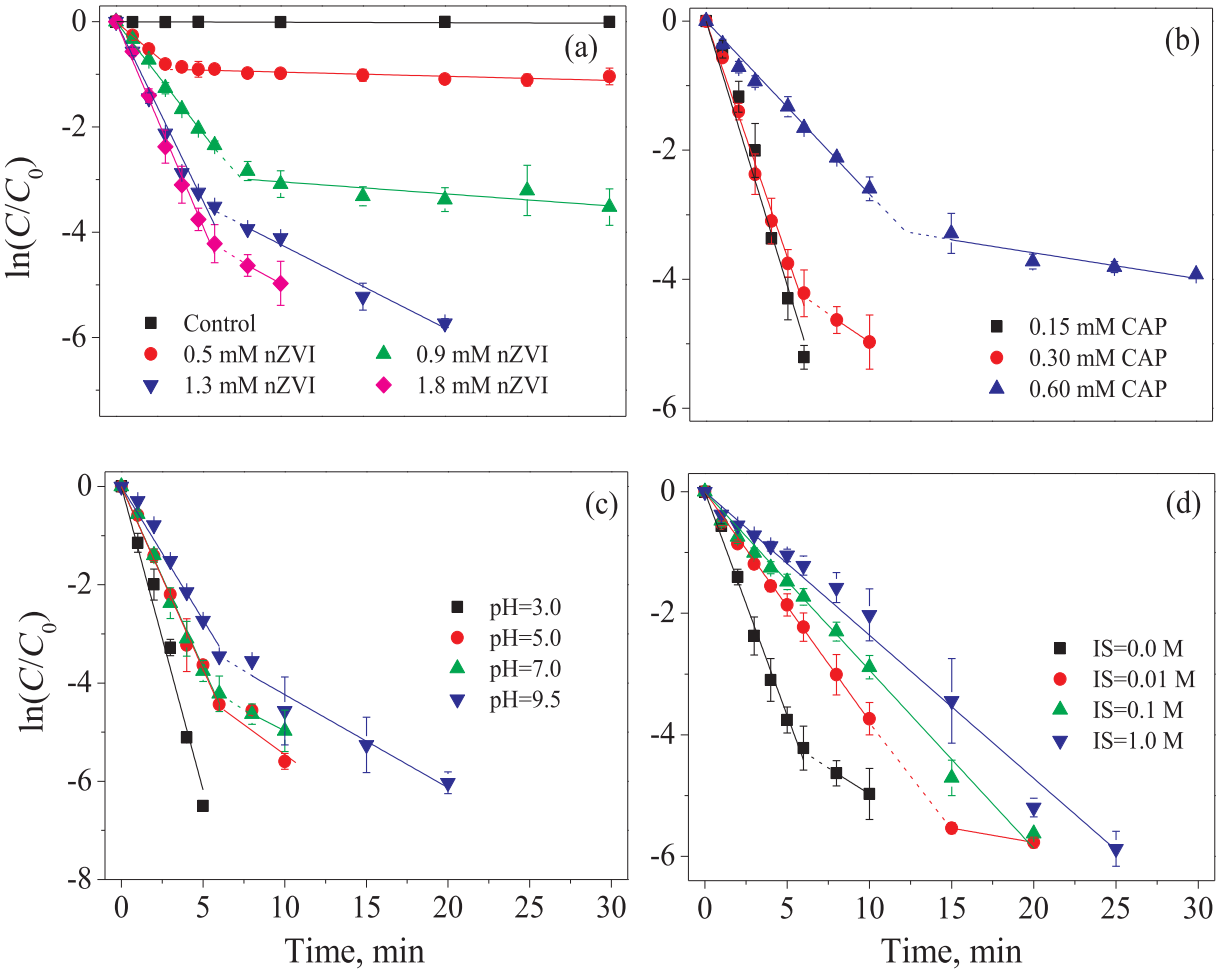

Fig. 4. Effects of (a) nZVI dosage, (b) initial CAP concentration, (c) initial pH, and (d) IS on the kinetics of CAP removal by nZVI (basic conditions: T = 303 K, pH = 7.0, nZVI = 1.8 mM, and CAP = 0.30 mM; control: without nZVI).

Table 2
Kinetics parameters for the removal of aqueous CAP by nZVI (basic conditions: T = 303 K, pH = 7.0, nZVI = 1.8 mM, and CAP = 0.30 mM).

Factor		k_{obs} (min^{-1})	$t_{1/2}$ (min)	k_{SA} (L min^{-1} m^{-2})	R^2
nZVI (mM)	0.0	–	–	–	–
	0.5	0.27	2.62	1.38	0.999
	0.9	0.40	1.73	1.23	0.998
	1.3	0.64	1.08	1.40	0.991
	1.8	0.74	0.94	1.13	0.997
Initial CAP concentration (mM)	0.15	0.83	0.84	1.27	0.987
	0.30	0.74	0.94	1.13	0.997
	0.60	0.27	2.59	0.42	0.996
Initial pH	3.0	1.24	0.56	1.90	0.992
	5.0	0.75	0.93	1.15	0.998
	7.0	0.74	0.94	1.13	0.997
	9.5	0.54	1.28	0.83	0.991
IS (M)	0.0	0.74	0.94	1.13	0.997
	0.01	0.38	1.84	0.58	0.999
	0.1	0.29	2.37	0.44	0.997
	1.0	0.24	2.94	0.37	0.993
Temperature (K)	283	0.28	2.48	0.43	0.979
	293	0.41	1.68	0.63	0.994
	303	0.74	0.94	1.13	0.997
	313	1.28	0.54	1.96	0.999

the Fe^0 peak was still observed in XRD spectra after reaction (Fig. 2c), and the decreased rate in the second stage was mainly attributed to the inactivation by iron oxides, which also has been proved by the TEM images (Fig. 1d and f). The high surface-area-normalized reaction rate (k_{SA}, 1.13 L min^{-1} m^{-2}) along with the high capacity (1000 mg g^{-1}) of 1.8 mM nZVI suggests that nZVI is a very promising remediation material for CAP-contaminated water. When the aqueous CAP concentration was below the limit of quantitation (LOQ) of HPLC, the samples were further analyzed by UPLC, which has a much lower LOQ of 0.19 ng L^{-1}, as reported in our previous study [41]. No residual CAP was detected, which indicated that nZVI was also efficient for trace CAP removal.

The effects of initial CAP concentration on the kinetics of removal are shown in Fig. 4b. Relatively higher concentrations of CAP (0.15–0.60 mM) are used in this study to meet the analytical sensitivity of HPLC, and to better compare the experimental results with previous studies regarding the removal of antibiotics by nZVI and other methods [26,29,42,43]. The k_{SA} of CAP removal by nZVI was 1.27 L min^{-1} m^{-2}, 1.13 L min^{-1} m^{-2}, and 0.42 L min^{-1} m^{-2} with initial CAP concentrations of 0.15 mM, 0.30 mM, and 0.60 mM, respectively. Although the initial CAP removal rate was decreased at higher CAP concentrations as the reaction sites on nZVI became relatively limited, satisfactory removal efficiency was still reached. Approximately 98% of the 0.60 mM CAP was removed after 30 min.

3.3.2. *Effects of initial pH, IS, and reaction temperature*

The initial solution pH is another important factor that affects nZVI

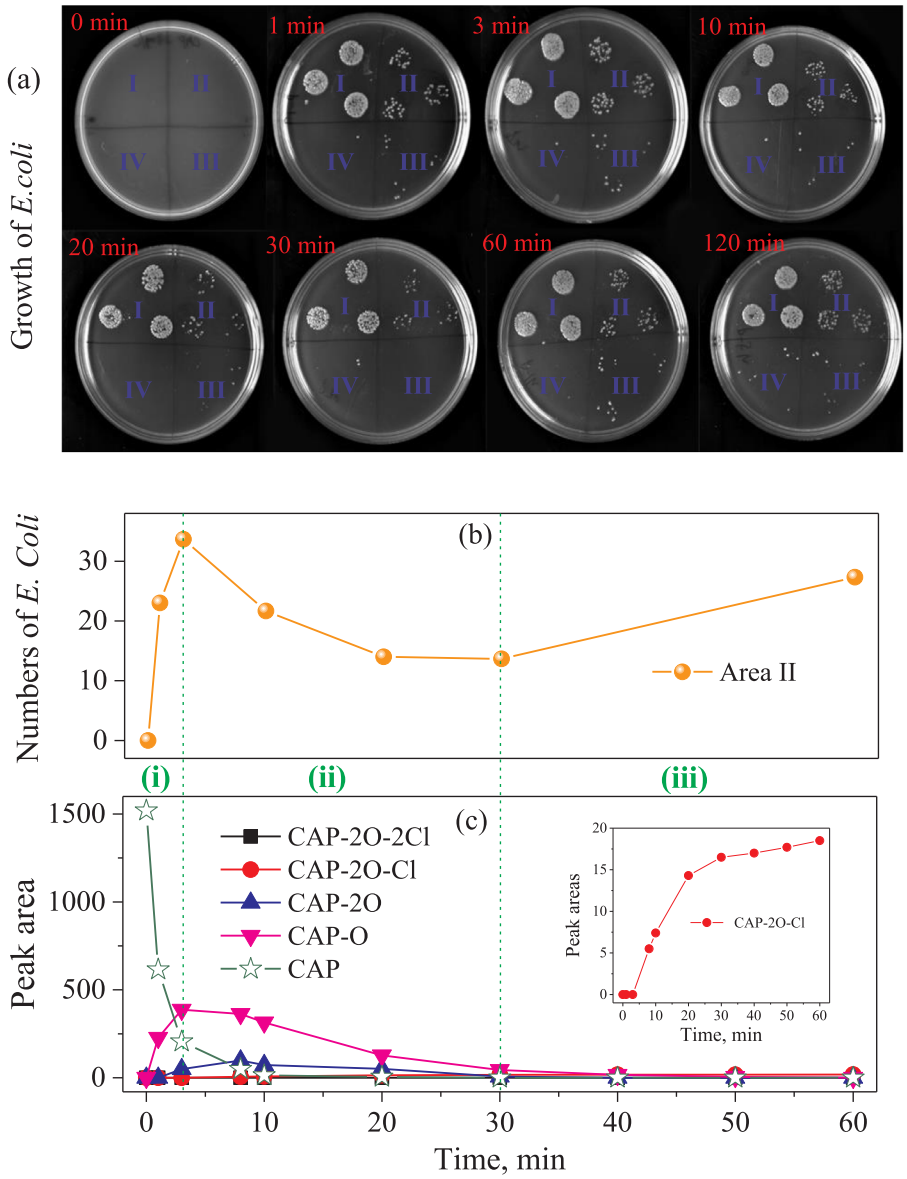

Fig. 5. Assessment of the antibacterial activity of the reaction solution under the basic conditions, (a) growth of *E. coli*, (b) number of *E. coli* in Area II, and (c) HPLC peak areas of CAP and its products.

reactivity toward aqueous contaminants [44–47]. As shown in Fig. 4c, the removal rate of CAP slightly decreased when the initial pH increased. Complete removal of CAP was achieved within 8 min at pH = 3.0, while complete CAP removal required 15 min, 20 min, and 30 min at pH = 5.0, 7.0, and 9.5, respectively. It has been widely reported that weak acidity (4.0–5.0) favors the removal of chlorinated organics and heavy metals by nZVI [48–51]. Generally, nZVI would be corroded too quickly under strongly acidic conditions (pH = 3.0), and excessive hydrogen would escape from the solution and lead to the low utilization ratio of Fe^0. However, unlike the removal of conventional pollutants by nZVI that usually requires several hours, the reactivity of nZVI toward CAP was very high, and only a few minutes were sufficient to remove most of the aqueous CAP. The rate of H_2 evolution by nZVI was reported to be 31 μmol $L\,g^{-1}\,h^{-1}$ [40], which could be ignored in the first few minutes. Thus, strong acidity would both favor the utilization ratio of Fe^0 and electron efficiency, and the highest rate of CAP removal by nZVI was observed at pH = 3.0 in this study, which is consistent with the removal of the antibiotic metronidazole by nZVI reported in previous study [35]. In addition, iron oxides and hydroxide would form a passive film on the nZVI surface in neutral and alkaline conditions and inhibit iron corrosion and contact with contaminants.

The background electrolyte concentration is also a basic parameter and can be represented by IS, which was adjusted by dissolving different amounts of NaCl in this study. It was observed that the removal rate of CAP decreased when the IS increased from 0.0 M to 1.0 M (Fig. 4d). The aggregation of nZVI would be favored by the increase of IS, which would gradually eliminate the repulsive particle-particle interactions due to double-layer compression [52,53]. The nZVI reactivity would be reduced due to the formation of larger nZVI aggregates. On the other hand, in the presence of both Cl^- and Fe^{2+}, akaganéite (β-FeOOH) rather than lepidocrocite was preferentially generated on the surface of nZVI, which would retard magnetite formation and iron corrosion [48,54]. The electron transfer between nZVI and CAP would be restrained by β-FeOOH, which would also result in a negative effect of IS on the removal of CAP by nZVI.

As shown in Fig. S11a, the removal rate of CAP by nZVI increased with increasing reaction temperature, which indicates that the reaction was endothermic. The 98% of CAP was removed with a removal rate of 1.96 L $min^{-1}\,m^{-2}$ in the first 3 min at 313 K. Additionally, a linear relationship between $\ln k_{obs}$ and $1/T$ was observed with a high correlation coefficient (R^2 = 0.988) in Fig. S11b. The experimental activation energy (E_a) of CAP removal by nZVI was 38 KJ mol^{-1}, which was

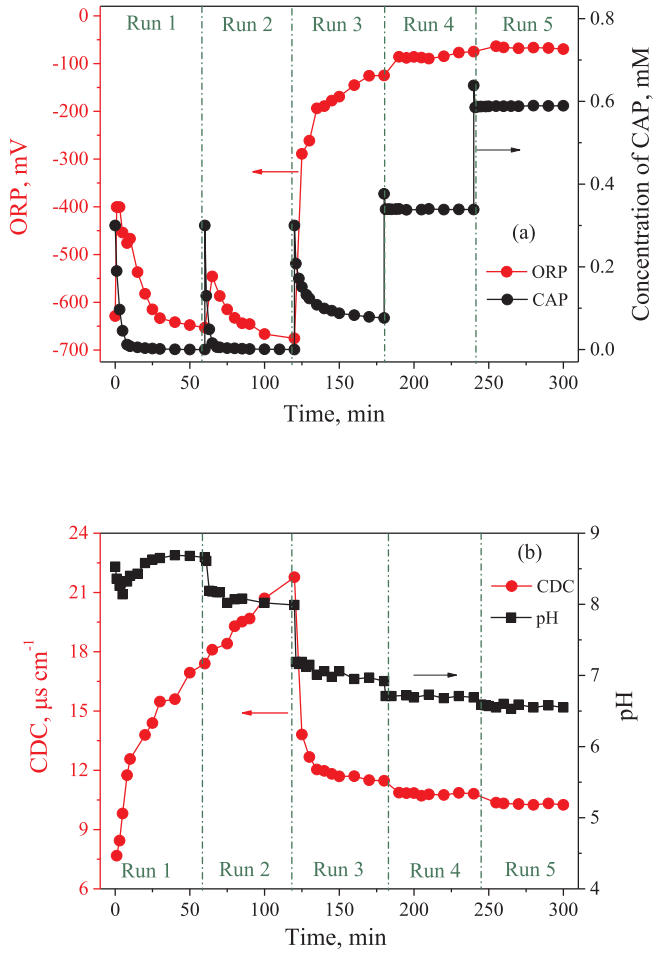

Fig. 6. Five consecutive cycles of CAP removal by nZVI, (a) CAP and ORP, (b) pH and CDC (T = 303 K, pH = 7.0, nZVI dosage = 0.18 mM, 0.30 mM CAP added at the beginning of each run).

lower than 45 KJ mol^{-1} for the degradation of perchloroethylene (PCE) by nZVI, and higher than 29 KJ mol^{-1} and 31 KJ mol^{-1} for pentachlorophenol (PCP) and PCE by Pd/Fe bimetallic nanoparticles, respectively [23,55].

3.4. Assessment of antibacterial activity of CAP and its reduction products

The antibacterial activity of CAP and its reduction products was evaluated using *E. coli*. Plates without contaminant and filtrate (blank experiment) and with filtrate of 0.1 g L^{-1} bare nZVI suspension without contaminant were used to investigate effects of iron ions on the toxicity, and ~46 ± 1 and 49 ± 2 *E. coli* grew in the mediums, respectively. This suggests that the toxicity from iron ions was negligible. Fig. 5a shows the variations in the growth of *E. coli* with reaction time. No *E. coli* grew in CAP solution at 0 min, while *E. coli* grew well with a high initial *E. coli* concentration (area I, 10^5 cfu) after the solution was treated by nZVI. More clear trends of the antibacterial activity of the reaction solution can be observed in area II (10^6 cfu) and III (10^7 cfu) with higher dilution times, and the numbers of *E. coli* in area II are shown in Fig. 5b. It was observed that the toxicity of the reaction solution followed a trend of "first decreased-then increased-then decreased", which could be explained by the evolution of the reaction products based on the MS signals (Fig. 5c).

In Period (i) (0–3 min), 90.5% of the CAP was removed, and the CAP – O (307) signal and the number of *E. coli* both reached a peak. The toxicity trend of "first decreased" is probably a result of the rapid removal of CAP, which had a high antibacterial activity. It has been reported that CAP and CAP – O (307) have much higher antibacterial activity than both CAP – 2O (293) and CAP – 2O – Cl (259) [26,56,57]. However, it was unexpected that the number and the growth of *E. coli* decreased with the degradation of CAP and CAP – O (307) and generation of CAP – 2O (293) and CAP – 2O – Cl (259) during Period (ii) (3–30 min). The increased antibacterial activity might be attributed to the synergistic effect of the co-existed CAP and its products. In Period (iii) (30–60 min), almost all the CAP and the CAP – O (307) product were removed with the completion of denitration and continuing dechlorination, which resulted in the decrease of antibacterial activity of the reaction solution. The elimination of antibacterial activity from CAP-containing wastewaters by nZVI has ecological significance in reducing the antibiotic selection pressure that results in the generation of antibiotic resistance genes and resistant bacteria in water-filled environments [26,58].

Table 3
Removal of CAP by nZVI in different water matrices (T = 303 K, initial CAP concentration = 0.30 mM, nZVI dosage = 1.8 mM, 30 min reaction).

Water	DI water	Ground water	River water	Sea water	Waste water
pH	7.0	7.6	7.2	8.1	7.8
ORP (mV)	1.36×10^2	8.97×10	1.17×10^2	7.76×10	1.16×10^2
Conductivity (μS cm^{-1})	1.12×10^0	1.09×10^3	5.43×10^2	1.49×10^4	4.62×10^2
Salinity (‰)	n.d.	5.70×10^{-1}	2.80×10^{-1}	9.20×10^0	2.30×10^{-1}
TOC (mg L^{-1})	n.d.	1.26	3.96	3.60	4.13
A_{254nm}	n.d.	1.60×10^{-2}	1.37×10^{-2}	1.30×10^{-2}	6.80×10^{-2}
Na^+ (mg L^{-1})	n.d.	5.15×10	3.86×10	1.50×10^3	2.80×10
K^+ (mg L^{-1})	n.d.	2.87×10^0	7.38×10^0	1.53×10^2	9.50×10^0
Ca^{2+} (mg L^{-1})	n.d.	1.34×10^2	5.18×10	1.37×10^2	5.07×10
Mg^{2+} (mg L^{-1})	n.d.	2.96×10	10.0×10^0	2.80×10^2	9.81×10^0
Cl^- (mg L^{-1})	n.d.	2.31×10^2	5.72×10	5.22×10^3	4.01×10
F^- (mg L^{-1})	n.d.	2.42×10^{-1}	5.28×10^{-1}	n.d.	n.d.
NO_3^- (mg L^{-1})	n.d.	3.63×10	1.22×10	7.77×10^0	3.42×10
SO_4^{2-} (mg L^{-1})	n.d.	1.20×10^2	9.53×10	1.09×10^2	5.61×10
PO_4^{3-} (mg L^{-1})	n.d.	4.03×10^{-1}	4.65×10^{-1}	4.29×10^{-1}	5.14×10^{-1}
Removal efficiency	100%	92.0%	93.7%	96.8%	87.9%
Pseudo-first-order parameters of the first stage reaction					
k_{obs} (min^{-1})	0.74	0.83	0.48	1.12	0.45
$t_{1/2}$ (min)	0.94	0.84	1.43	0.62	1.54
k_{SA} (L min^{-1} m^{-2})	1.13	1.27	0.74	1.72	0.69
R^2	0.997	0.987	0.980	0.990	0.988

n.d.: not detected.

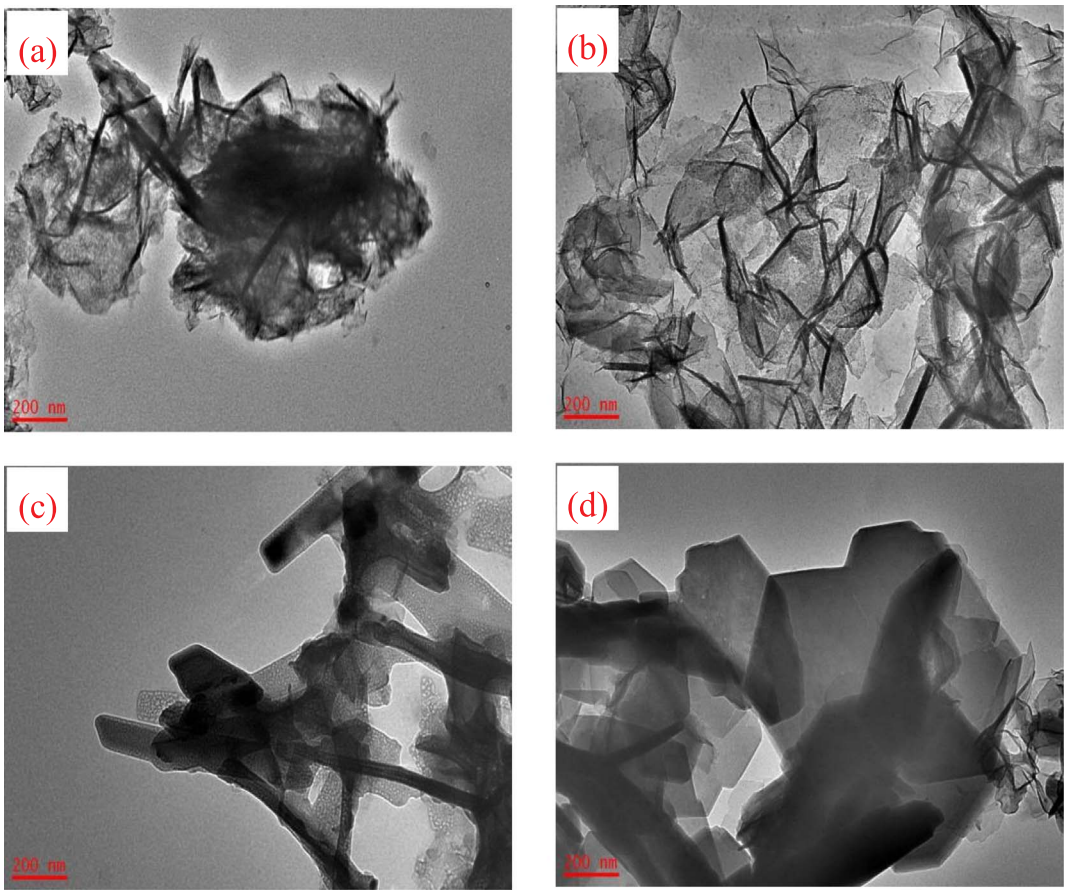

Fig. 7. TEM images of nZVI after the reaction with CAP in (a) groundwater, (b) river water, (c) sea water, and (d) wastewater (T = 303 K, initial CAP concentration = 0.30 mM, nZVI dosage = 1.8 mM, 30 min reaction).

3.5. Five consecutive cycles of CAP removal by nZVI

The reusability of nZVI was investigated by adding consecutive doses of 0.30 mM CAP and allowing 60 min reaction time between doses. As shown in Fig. 6a, 100%, 100%, 75%, 12%, and 9% of CAP was removed by nZVI in each run, respectively. The decreased removal was mainly attributed to the consumption of nZVI. Some water chemistry indicators of can also be used to evaluate the nZVI reactivity and explain the decreased removal [59]. ORP is a measure of electron activity in a solution and indicates its relative tendency to accept or transfer electrons [60]. A highly reducing condition of approximately −630 mV ORP was obtained after the addition of nZVI (Fig. 6a). This value was sharply increased upon adding CAP, and then trended to drop back due to the rapid removal of CAP by nZVI. However, the ORP value did not come back after CAP addition at run 3, indicated the exhaust of Fe^0 in the solution. After the particle was exhausted, almost no CAP was reduced except a small portion of adsorption by the nanoparticles in run 4 and 5 as the reaction products did not increase during these two runs. Similar changes of ORP after the addition of nZVI and contaminant were observed in previous studies [61].

The results are also consistent with changes of the solution pH and conductivity (CDC) (Fig. 6b). The pH increased to around 8.5 after the addition of nZVI as the corrosion of nZVI consumes protons. The pH value decreased upon adding CAP and then maintained almost constant during each run. The solution CDC was gradually increased in the first two runs due to the dissolved Fe^{2+} via the corrosion of Fe^0. Note that the CDC and pH decreased sharply along with the increase of ORP in run 3, which indicates that the dissolved Fe was precipitated with OH^-, and the reductive Fe^0 and Fe^{2+} were quickly consumed.

3.6. Performance of nZVI in CAP removal in different water matrices

Batch experiments were performed to investigate the potential application of nZVI for CAP removal in different water matrices, including groundwater, river water, seawater, and wastewater. The important properties and compositions of these water types are shown in Table 3. After reacting for 30 min, the removal efficiency of CAP in groundwater, river water, seawater, and wastewater was 92.0%, 93.7%, 96.8%, and 87.9%, respectively. The CAP removal kinetics could also be divided into two stages as in these waters (Fig. S12). The duration of the first stage (3 min) was shorter than that in DI water (6 min), and then the CAP removal rate slowed significantly. No obvious removal of CAP was observed in the second stage. The results indicate that the reactivity of nZVI was high in the first several minutes and then quickly decreased due to the complete consumption of Fe^0 in the complex water environments. As shown in Table 3, the first stage of CAP removal also followed the pseudo-first-order kinetics model. The values of k_{SA} in the wastewater (0.69 L min^{-1} m^{-2}) and river water (0.74 L min^{-1} m^{-2}) were smaller than those in DI water (1.13 L min^{-1} m^{-2}), while the values of k_{SA} in the seawater (1.72 L min^{-1} m^{-2}) and groundwater (1.27 L min^{-1} m^{-2}) were even larger. It was not expected that nZVI still had high reactivity with CAP in seawater. According to the higher conductivity and salinity, the IS of seawater was estimated to be much higher than other water matrices in this study, resulting in serious aggregation of nZVI with an average size of several micrometers (Fig. S13) and decrease of reactivity. The higher removal efficiency of CAP in seawater than other water matrices might be attributed the lower ORP of seawater that would favor the electron transfer and the lower concentration of reducible NO_3^- that could decrease the competition of electrons with CAP.

Since the product standards could not be obtained, HPCL peak areas of CAP and intermediates/products detected in the same batch were used to describe the product distribution in different waters (Fig. S14). It was observed that the product distributions were similar. As the reaction proceeded, CAP sharply decreased in the first few minutes, intermediate products (CAP − O and CAP − 2O) followed a trend of first increased then decreased, and product CAP − 2O − Cl gradually increased while product CAP − 2O − 2Cl was not detected. Satisfactory removal of CAP by nZVI was achieved in different water matrices, and practical applications could be expected after modifying nZVI and optimizing the operating conditions.

TEM analysis was further performed to investigate the corrosion of nZVI after reaction with CAP in different water matrices. The needle-like substance in the TEM images of nZVI after reaction with CAP in the river water and groundwater (Fig. 7a and b) was probably goethite (α-FeOOH) according to several previous studies [62,63], α-FeOOH was also reported to be a major mineral phase yielded from the reaction between nZVI and contaminants in water [64]. Fig. 7c suggested that nZVI was transformed to akaganéite (β-FeOOH) like substance after reaction in the sea water [65], which was widely accepted to be one of the main products of iron corrosion in marine environments [54]. Both lepidocrocite (γ-FeOOH) and green rust ($(Fe_2(OH,SO_4)_{4.88})$ like structures were observed in the TEM image of nZVI after reaction with CAP in the wastewater (Fig. 7d) [66]. Green rust is most likely formed in a reduced environment, and usually accompanies with γ-FeOOH and also formed via the reduction of γ-FeOOH [67,68].

4. Conclusions

nZVI was prepared, characterized, and employed to effectively remove the antibiotic CAP from water. A core-shell structure of nZVI was suggested by various characterization methods. Larger nZVI dosages and higher reaction temperatures promoted the removal of CAP, while higher initial solution pH and IS had negative effects. Based on the fitting of experimental data via a pseudo-first-order kinetic model, the entire reaction process could be divided into two stages: ultrafast and gradual removal, which was probably attributed to the consumption of Fe^0 and inactivation of nZVI. The reaction products were carefully analyzed and identified as CAP − O, CAP − 2O, CAP − 2O − Cl, and CAP − 2O − 2Cl using HPLC, UPLC-MS/MS, and NMR-H. The nitro reduction and dechlorination of CAP occurred successively, resulting in decreased antibacterial activity of the residual solution. Moreover, CAP could be efficiently removed in different natural waters, mainly via the strong reactivity of nZVI in the first several minutes. For future studies, further improvements of nZVI are required in order to inhibit inactivation at late stage and maintain particle longevity.

Acknowledgements

The authors would like to acknowledge the Shanghai Pujiang Program (No. 15PJD014), Chenguang Program of Shanghai Education Development Foundation and Shanghai Municipal Education Commission (No. 16CG23), the National Key Research and Development Program of China (2016YFC0402600), and the National Natural Science Foundation of China (No. 41522111) for their financial support.

Appendix A. Supplementary data

Supplementary data associated with this article can be found, in the online version, at http://dx.doi.org/10.1016/j.cej.2017.10.060.

References

[1] B. Petrie, R. Barden, B. Kasprzyk-Hordern, A review on emerging contaminants in wastewaters and the environment: Current knowledge, understudied areas and recommendations for future monitoring, Water Res. 72 (2015) 3–27.
[2] M.B. Ahmed, J.L. Zhou, H.H. Ngo, W. Guo, Adsorptive removal of antibiotics from water and wastewater: progress and challenges, Sci. Total Environ. 532 (2015) 112–126.
[3] R. Hao, R. Zhao, S. Qiu, L. Wang, H. Song, Antibiotics crisis in China, Science 348 (2015) 1100.
[4] H.W. Leung, T.B. Minh, M.B. Murphy, J.C.W. Lam, M.K. So, M. Martin, P.K.S. Lam, B.J. Richardson, Distribution, fate and risk assessment of antibiotics in sewage treatment plants in Hong Kong, South China, Environ. Int. 42 (2012) 1–9.
[5] Q. Sui, J. Huang, S. Deng, G. Yu, Q. Fan, Occurrence and removal of pharmaceuticals, caffeine and DEET in wastewater treatment plants of Beijing, China, Water Res. 44 (2010) 417–426.
[6] X. Hu, Q. Zhou, Y. Luo, Occurrence and source analysis of typical veterinary antibiotics in manure, soil, vegetables and groundwater from organic vegetable bases, northern China, Environ. Pollut. 158 (2010) 2992–2998.
[7] C. Yan, Y. Yang, J. Zhou, M. Nie, M. Liu, M.F. Hochella Jr., Selected emerging organic contaminants in the Yangtze Estuary, China: a comprehensive treatment of their association with aquatic colloids, J. Hazard. Mater. 283 (2015) 14–23.
[8] H. Liu, G. Zhang, C. Liu, L. Li, M. Xiang, The occurrence of chloramphenicol and tetracyclines in municipal sewage and the Nanming River, Guiyang City, China, J. Environ. Monitor. 11 (2009) 1199–1205.
[9] H. Zhao, X. Liu, Z. Cao, Y. Zhan, X. Shi, Y. Yang, J. Zhou, J. Xu, Adsorption behavior and mechanism of chloramphenicols, sulfonamides, and non-antibiotic pharmaceuticals on multi-walled carbon nanotubes, J. Hazard. Mater. 310 (2016) 235–245.
[10] F. Chen, Q. Yang, J. Sun, F. Yao, S. Wang, Y. Wang, X. Wang, X. Li, C. Niu, D. Wang, G. Zeng, Enhanced photocatalytic degradation of tetracycline by AgI/$BiVO_4$ heterojunction under visible-light irradiation: mineralization efficiency and mechanism, ACS Appl. Mater. Inter. 8 (2016) 32887–32900.
[11] D. Qin, W. Lu, X. Wang, N. Li, X. Chen, Z. Zhu, W. Chen, Graphitic carbon nitride from burial to re-emergence on polyethylene terephthalate nanofibers as an easily recycled photocatalyst for degrading antibiotics under solar irradiation, ACS Appl. Mater. Inter. 8 (2016) 25962–25970.
[12] W. Tian, H. Zhang, X. Duan, H. Sun, M.O. Tade, H.M. Ang, S. Wang, Nitrogen- and sulfur-codoped hierarchically porous carbon for adsorptive and oxidative removal of pharmaceutical contaminants, ACS Appl. Mater. Inter. 8 (2016) 7184–7193.
[13] Q. Liu, L. Zhong, Q. Zhao, C. Frear, Y. Zheng, Synthesis of Fe_3O_4/polyacrylonitrile composite electrospun nanofiber mat for effective adsorption of tetracycline, ACS Appl. Mater. Inter. 7 (2015) 14573–14583.
[14] J. Xue, S. Ma, Y. Zhou, Z. Zhang, M. He, Facile photochemical synthesis of Au/Pt/g-C_3N_4 with plasmon-enhanced photocatalytic activity for antibiotic degradation, ACS Appl. Mater. Inter. 7 (2015) 9630–9637.
[15] Y. Hwang, D. Kim, H. Shin, Mechanism study of nitrate reduction by nano zero valent iron, J. Hazard. Mater. 185 (2011) 1513–1521.
[16] S. Li, W. Wang, F. Liang, W. Zhang, Heavy metal removal using nanoscale zero-valent iron (nZVI): theory and application, J. Hazard. Mater. 322 (2016) 163–171.
[17] J. Gao, W. Wang, A.J. Rondinone, F. He, L. Liang, Degradation of trichloroethene with a novel ball milled Fe–C nanocomposite, J. Hazard. Mater. 300 (2015) 443–450.
[18] Y. Liu, G.V. Lowry, Effect of particle age (Fe^0 content) and solution pH on NZVI reactivity: H_2 evolution and TCE dechlorination, Environ. Sci. Technol. 40 (2006) 6085–6090.
[19] J. Xu, X. Liu, G.V. Lowry, Z. Cao, H. Zhao, J.L. Zhou, X. Xu, Dechlorination mechanism of 2,4-dichlorophenol by magnetic MWCNTs supported Pd/Fe nanohybrids: rapid adsorption, gradual dechlorination, and desorption of phenol, ACS Appl. Mater. Inter. 8 (2016) 7333–7342.
[20] F. He, D. Zhao, C. Paul, Field assessment of carboxymethyl cellulose stabilized iron nanoparticles for in situ destruction of chlorinated solvents in source zones, Water Res. 44 (2010) 2360–2370.
[21] J. Xu, J. Tang, S.A. Baig, X. Lv, X. Xu, Enhanced dechlorination of 2,4-dichlorophenol by Pd/Fe-Fe_3O_4 nanocomposites, J. Hazard. Mater. 244–245 (2013) 628–636.
[22] Y. Shih, Y. Tai, Reaction of decabrominated diphenyl ether by zerovalent iron nanoparticles, Chemosphere 78 (2010) 1200–1206.
[23] Y. Shih, M. Chen, Y. Su, C. Tso, Concurrent oxidation and reduction of pentachlorophenol by bimetallic zerovalent Pd/Fe nanoparticles in an oxic water, J. Hazard. Mater. 301 (2016) 416–423.
[24] Y. Keum, Q.X. Li, Reductive debromination of polybrominated diphenyl ethers by zerovalent iron, Environ. Sci. Technol. 39 (2005) 2280–2286.
[25] C. Tso, Y. Shih, The reactivity of well-dispersed zerovalent iron nanoparticles toward pentachlorophenol in water, Water Res. 72 (2015) 372–380.
[26] B. Liang, H. Cheng, D. Kong, S. Gao, F. Sun, D. Cui, F. Kong, A. Zhou, W. Liu, N. Ren, W. Wu, A. Wang, D. Lee, Accelerated reduction of chlorinated nitroaromatic antibiotic chloramphenicol by biocathode, Environ. Sci. Technol. 47 (2013) 5353–5361.
[27] M. Sun, D.D. Reible, G.V. Lowry, K.B. Gregory, Effect of applied voltage, initial concentration, and natural organic matter on sequential reduction/oxidation of nitrobenzene by graphite electrodes, Environ. Sci. Technol. 46 (2012) 6174–6181.
[28] K.P. Singh, A.K. Singh, S. Gupta, P. Rai, Modeling and optimization of reductive degradation of chloramphenicol in aqueous solution by zero-valent bimetallic nanoparticles, Environ. Sci. Pollut. R. 19 (2012) 2063–2078.
[29] S. Xia, Z. Gu, Z. Zhang, J. Zhang, S.W. Hermanowicz, Removal of chloramphenicol from aqueous solution by nanoscale zero-valent iron particles, Chem. Eng. J. 257 (2014) 98–104.
[30] J. Xu, X. Lv, J. Li, Y. Li, L. Shen, H. Zhou, X. Xu, Simultaneous adsorption and dechlorination of 2,4-dichlorophenol by Pd/Fe nanoparticles with multi-walled carbon nanotube support, J. Hazard. Mater. 225–226 (2012) 36–45.

[31] M. Liu, Y. Wang, L. Chen, Y. Zhang, Z. Lin, $Mg(OH)_2$ supported nanoscale zero valent iron enhancing the removal of Pb(II) from aqueous solution, ACS Appl. Mater. Inter. 7 (2015) 7961–7969.
[32] B. Sunkara, J. Zhan, J. He, G.L. McPherson, G. Piringer, V.T. John, Nanoscale zerovalent iron supported on uniform carbon microspheres for the in situ remediation of chlorinated hydrocarbons, ACS Appl. Mater. Inter. 2 (2010) 2854–2862.
[33] E. Kim, J. Kim, A. Azad, Y. Chang, Facile synthesis and characterization of Fe/FeS nanoparticles for environmental applications, ACS Appl. Mater. Inter. 3 (2011) 1457–1462.
[34] S. Bae, W. Lee, Influence of riboflavin on nanoscale zero-valent iron reactivity during the degradation of carbon tetrachloride, Environ. Sci. Technol. 48 (2014) 2368–2376.
[35] Z. Fang, J. Chen, X. Qiu, X. Qiu, W. Cheng, L. Zhu, Effective removal of antibiotic metronidazole from water by nanoscale zero-valent iron particles, Desalination 268 (2011) 60–67.
[36] A. Ghauch, A. Tuqan, H.A. Assi, Antibiotic removal from water: elimination of amoxicillin and ampicillin by microscale and nanoscale iron particles, Environ. Pollut. 157 (2009) 1626–1635.
[37] J. Xu, Z. Cao, X. Liu, H. Zhao, X. Xiao, J. Wu, X. Xu, J.L. Zhou, Preparation of functionalized Pd/Fe-Fe_3O_4@MWCNTs nanomaterials for aqueous 2,4-dichlorophenol removal: Interactions, influence factors, and kinetics, J. Hazard. Mater. 317 (2016) 656–666.
[38] J. Tang, L. Tang, H. Feng, G. Zeng, H. Dong, C. Zhang, B. Huang, Y. Deng, J. Wang, Y. Zhou, pH-dependent degradation of p-nitrophenol by sulfidated nanoscale zerovalent iron under aerobic or anoxic conditions, J. Hazard. Mater. 320 (2016) 581–590.
[39] Z. Cao, X. Liu, J. Xu, J. Zhang, Y. Yang, J. Zhou, X. Xu, G.V. Lowry, Removal of antibiotic florfenicol by sulfide-modified nanoscale zero-valent iron, Environ. Sci. Technol. 51 (2017) 11269–11277.
[40] Y. Liu, S.A. Majetich, R.D. Tilton, D.S. Sholl, G.V. Lowry, TCE dechlorination rates, pathways, and efficiency of nanoscale iron particles with different properties, Environ. Sci. Technol. 39 (2005) 1338–1345.
[41] H. Zhao, J.L. Zhou, J. Zhang, Tidal impact on the dynamic behavior of dissolved pharmaceuticals in the Yangtze Estuary, China, Sci. Total Environ. 536 (2015) 946–954.
[42] H. Chen, H. Luo, Y. Lan, T. Dong, B. Hu, Y. Wang, Removal of tetracycline from aqueous solutions using polyvinylpyrrolidone (PVP-K30) modified nanoscale zero valent iron, J. Hazard. Mater. 192 (2011) 44–53.
[43] N. Liu, S. Sijak, M. Zheng, L. Tang, G. Xu, M. Wu, Aquatic photolysis of florfenicol and thiamphenicol under direct UV irradiation, UV/H_2O_2 and UV/Fe(II) processes, Chem. Eng. J. 260 (2015) 826–834.
[44] X. Zhao, W. Liu, Z. Cai, B. Han, T. Qian, D. Zhao, An overview of preparation and applications of stabilized zero-valent iron nanoparticles for soil and groundwater remediation, Water Res. 100 (2016) 245–266.
[45] Y. Sun, J. Li, T. Huang, X. Guan, The influences of iron characteristics, operating conditions and solution chemistry on contaminants removal by zero-valent iron: a review, Water Res. 100 (2016) 277–295.
[46] B. Calderon, A. Fullana, Heavy metal release due to aging effect during zero valent iron nanoparticles remediation, Water Res. 83 (2015) 1–9.
[47] Y. Zhou, L. Tang, G. Yang, G. Zeng, Y. Deng, B. Huang, Y. Cai, J. Tang, J. Wang, Y. Wu, Phosphorus-doped ordered mesoporous carbons embedded with Pd/Fe bimetal nanoparticles for the dechlorination of 2,4-dichlorophenol, Catal. Sci. Technol. 6 (2016) 1930–1939.
[48] J. Xu, L. Tan, S.A. Baig, D. Wu, X. Lv, X. Xu, Dechlorination of 2,4-dichlorophenol by nanoscale magnetic Pd/Fe particles: Effects of pH, temperature, common dissolved ions and humic acid, Chem. Eng. J. 231 (2013) 26–35.
[49] J. Xu, T. Sheng, Y. Hu, S.A. Baig, X. Lv, X. Xu, Adsorption-dechlorination of 2,4-dichlorophenol using two specified MWCNTs-stabilized Pd/Fe nanocomposites, Chem. Eng. J. 219 (2013) 162–173.
[50] S. Luo, T. Lu, L. Peng, J. Shao, Q. Zeng, J. Gu, Synthesis of nanoscale zero-valent iron immobilized in alginate microcapsules for removal of Pb(II) from aqueous solution, J. Mater. Chem. A 2 (2014) 15463–15472.
[51] F. Liu, C. Shan, X. Zhang, Y. Zhang, W. Zhang, B. Pan, Enhanced removal of EDTA-chelated Cu(II) by polymeric anion-exchanger supported nanoscale zero-valent iron, J. Hazard. Mater. 321 (2017) 290–298.
[52] M. Basnet, C.D. Tommaso, S. Ghoshal, N. Tufenkji, Reduced transport potential of a palladium-doped zero valent iron nanoparticle in a water saturated loamy sand, Water Res. 68 (2015) 354–363.
[53] M. Basnet, S. Ghoshal, N. Tufenkji, Rhamnolipid biosurfactant and soy protein act as effective stabilizers in the aggregation and transport of palladium-doped zerovalent iron nanoparticles in saturated porous media, Environ. Sci. Technol. 47 (2013) 13355–13364.
[54] C. Rémazeilles, P. Refait, On the formation of β-FeOOH (akaganéite) in chloride-containing environments, Corros. Sci. 49 (2007) 844–857.
[55] H. Lien, W. Zhang, Nanoscale Pd/Fe bimetallic particles: catalytic effects of palladium on hydrodechlorination, Appl. Catal. B-Environ. 77 (2007) 110–116.
[56] A.L. Smith, A.L. Erwin, T. Kline, W.C.T. Unrath, K. Nelson, A. Weber, W.N. Howald, Chloramphenicol is a substrate for a novel nitroreductase pathway in haemophilus influenzae, Antimicrob. Agents Ch. 51 (2007) 2820–2829.
[57] B.J. Gross, R.V. Branchflower, T.R. Burke, D.E. Lees, L.R. Pohl, Bone marrow toxicity in vitro of chloramphenicol and its metabolites, Toxicol. Appl. Pharm. 64 (1982) 557–565.
[58] X. Zhang, T. Zhang, H.H.P. Fang, Antibiotic resistance genes in water environment, Appl. Microbiol. Biot. 82 (2009) 397–414.
[59] R. Yu, F. Chi, W. Cheng, J. Chang, Application of pH, ORP, and DO monitoring to evaluate chromium(VI) removal from wastewater by the nanoscale zero-valent iron (nZVI) process, Chem. Eng. J. 255 (2014) 568–576.
[60] D.W. Elliott, W. Zhang, Field assessment of nanoscale bimetallic particles for groundwater treatment, Environ. Sci. Technol. 35 (2001) 4922–4926.
[61] S. Bae, K. Hanna, Reactivity of nanoscale zero-valent iron in unbuffered systems: Effect of pH and Fe(II) dissolution, Environ. Sci. Technol. 49 (2015) 10536–10543.
[62] J.H. Strehlau, J.D. Schultz, A.M. Vindedahl, W.A. Arnold, R.L. Penn, Effect of nonreactive kaolinite on 4-chloronitrobenzene reduction by Fe(II) in goethite-kaolinite heterogeneous suspensions, Environ. Sci. Nano 4 (2017) 325–334.
[63] A.M. Stemig, T.A. Do, V.M. Yuwono, W.A. Arnold, R.L. Penn, Goethite nanoparticle aggregation: effects of buffers, metal ions, and 4-chloronitrobenzene reduction, Environ. Sci. Nano 1 (2014) 478–487.
[64] H. Kim, J. Ahn, K. Hwang, I. Kim, I. Hwang, Atmospherically stable nanoscale zero-valent iron particles formed under controlled air contact: characteristics and reactivity, Environ. Sci. Technol. 44 (2010) 1760–1766.
[65] J. Kim, W. Li, B.L. Philips, C.P. Grey, Phosphate adsorption on the iron oxyhydroxides goethite ([small alpha]-FeOOH), akaganeite ([small beta]-FeOOH), and lepidocrocite ([gamma]-FeOOH): a 31P NMR study, Energ. Environ. Sci. 4 (2011) 4298–4305.
[66] O. Larsen, D. Postma, Kinetics of reductive bulk dissolution of lepidocrocite, ferrihydrite, and goethite, Geochim. Cosmochim. Ac. 65 (2001) 1367–1379.
[67] M. Baalousha, Y. Yang, M.E. Vance, B.P. Colman, S. McNeal, J. Xu, J. Blaszczak, M. Steele, E. Bernhardt, M.F. Hochella Jr., Outdoor urban nanomaterials: The emergence of a new, integrated, and critical field of study, Sci. Total Environ. 557–558 (2016) 740–753.
[68] C.A. Johnson, M. Murayama, K. Küsel, M.F. Hochella Jr., Polycrystallinity of green rust minerals and their synthetic analogs: Implications for particle formation and reactivity in complex systems, Am. Mineral. 100 (2015) 2091–2105.